Applied Surface Science 279 (2013) 432–440

Contents lists available at SciVerse ScienceDirect

Applied Surface Science

journal homepage: www.elsevier.com/locate/apsusc

Adsorption characteristics and behaviors of graphene oxide for Zn(II) removal from aqueous solution

Hou Wang[a,b], Xingzhong Yuan[a,b,*], Yan Wu[c], Huajun Huang[a,b], Guangming Zeng[a,b], Yan Liu[a,b], Xueli Wang[a,b], Ningbo Lin[a,b], Yu Qi[d]

[a] College of Environmental Science and Engineering, Hunan University, Changsha 410082, PR China
[b] Key Laboratory of Environment Biology and Pollution Control, Hunan University, Ministry of Education, Changsha 410082, PR China
[c] College of Environment and Energy, South China University of Technology, Guangzhou 510006, PR China
[d] Civil and Environmental Engineering, Carnegie Mellon University, Pittsburgh 15213, United States

ARTICLE INFO

Article history:
Received 10 January 2013
Received in revised form 24 April 2013
Accepted 25 April 2013
Available online 6 May 2013

Keywords:
Graphene oxide
Adsorption
Kinetics
Zinc

ABSTRACT

In this study, graphene oxide (GO) was synthesized via modified Hummers' method, and characterized by scanning electron microscopy (SEM), atomic force microscope (AFM), X-ray diffraction (XRD), and Fourier transform infrared spectrum (FT-IR), X-ray photoelectron spectroscopy (XPS). The adsorption of Zn(II) on GO as a function of pH, adsorbent dosage, foreign ions, contact time, and temperature was investigated using batch technique. Results showed that the suitable pH for Zn(II) removal was about 7.0, and the optimal dosage was 2 mg. The adsorption of Zn(II) onto GO increased sharply within 20 min and obtained equilibrium gradually. Meanwhile, foreign ion and temperature also affected the adsorption performance of GO. The adsorption process was found to be well described by the pseudo-second-order rate model. Equilibrium studies indicated that the data of Zn(II) adsorption followed the Langmuir model. The maximum adsorption capacity for Zn(II) was up to 246 mg/g with a Langmuir adsorption equilibrium constant of 5.7 L/g at 20 °C. The thermodynamic parameters calculated from temperature-dependent sorption isotherms suggested that Zn(II) sorption on GO was an exothermic and spontaneous process in nature. The possibility of Zn(II) recovery was investigated and the result revealed that the maximum Zn(II) recovery yield was achieved with hydrochloric acid.

1. Introduction

With the intensive spread and accumulation of contaminants in water and sediment, water pollution caused by heavy metal ions has currently attracted fastidious concern due to their toxic effect to human health and other organisms in the environment [1]. Excess heavy metals are discharged into the aqueous environment through various sources including metal smelters, effluents from plastics, paper industries, microelectronics, mining operations, usage of fertilizers and pesticides [2]. Zinc is one of the most significant heavy metals often found in different effluents and travels through the food chain via bioaccumulation [3]. Although zinc is considered as an essential micronutrient for life, it can be toxic beyond permissible limits. The World Health Organization recommends that the maximum acceptable concentration of zinc in drinking water is 5 mg/L [4]. Acute exposure to Zn(II) can lead to stomach cramps, skin irritations, vomiting, nausea and anemia [5].

To date, zinc removal techniques include chemical precipitation, electrochemical treatment, ion exchange, membrane separation, adsorption, etc. [6]. Generally, adsorption has been and still is the most often used and studied method because it is cheap, effective and easy-adaption [7,8]. A lot of materials such as biomass [9], carbon nano-materials [10–12], active carbon [13], bentonite [6], resin [14], and carbon nano-materials [15], are well-known for efficient removal of Zn(II) from aqueous solution. Among them, graphene-based materials are the most effective with high adsorption capacity and excellent performance [7,16].

Graphene, a new two-dimensional carbon nanomaterial, a fundamental building block for graphitic materials, has been the hotspot in multidisciplinary field owing to its large surface area, excellent electrical, thermal and mechanical properties [17,18]. Graphene oxide, which is considered as oxidized form of graphene, contains a range of reactive oxygen functional groups, e.g. epoxides, hydroxyl, ketones, and carboxyl groups [19]. In addition, GO has high surface area up to 2620 m^2/g (theoretical value) and can be readily obtained from cheap natural graphite in large scale [20]. From these viewpoints, GO is served as a suitable adsorbent for

* Corresponding author at: College of Environmental Science and Engineering, Hunan University, Changsha 410082, PR China. Tel.: +86 731 88821413; fax: +86 731 88823701.
E-mail address: yxz@hnu.edu.cn (X. Yuan).

0169-4332/$ – see front matter © 2013 Elsevier B.V. All rights reserved.
http://dx.doi.org/10.1016/j.apsusc.2013.04.133

the sequestration and removal of pollutants in water. Recently, many literature demonstrate that the synthetic GO has high adsorption capability toward dyes [21], pharmaceutical antibiotics [22], and heavy metals [23,24]. However, systematic studies on zinc adsorption characteristics and behaviors onto GO under various physicochemical parameters are limited and even not involved.

In this study, different experimental conditions, involving pH, adsorbent dose, foreign ions, contact time, and temperature, are investigated to understand the adsorption characteristics for the removal of Zn(II) from aqueous solution by the use of GO. Meanwhile, behaviors and mechanisms of Zn(II) adsorption are comprehensively explored by adsorption kinetics, isotherm models and thermodynamic parameters. Ultimately, the preliminary desorption study is conducted to investigate the possibility of recycling GO and Zn(II) ion recovery.

2. Materials and methods

2.1. Materials

GO was synthesized via modified Hummers' method [25] from the powder graphite (particle size ≤ 30 mm, Tianjing Kermel Chemical Regent Ltd., China). Briefly, layered graphite was oxidized by concentrated H_2SO_4 and $KMnO_4$. Then, the excess MnO_4^- in the suspension was eliminated by 30% H_2O_2 and the desired products were rinsed with HCl (10% v/v) and ultrapure water. Finally, with the help of ultrasonication, the oxide graphite layers were peeled off. More detailed processes had been reported in our previous research [26]. All chemicals were analytical grade and used without any further purification. All solutions were prepared using ultrapure water. The initial Zn(II) solution was prepared by dissolving $Zn(NO_3)_2$ in ultrapure water.

2.2. Characterization of graphene oxide

The obtained GO sample was characterized by SEM, XRD, AFM, FT-IR and XPS. SEM images were obtained using a emission scanning electron microscope (JSM-7001F, Japan). The XRD patterns were carried out with Bruker AXS D8 Advance diffractometer operating with Cu-K*a* source (λ = 1.541 Å). AFM image was acquired in ambient air with a tapping mode atomic force microscopy (SPI3800N-SPA400, Seiko Instrument). FT-IR spectroscopy measurements were conducted by using Nicolet 5700 Spectrometer in KBr pellet at room temperature. The surface elemental composition analyses were proposed based on the XPS spectra (Thermo Fisher Scientific, UK) with a resolution of 0.5 eV. The zeta potentials of GO dispersions were measured as a function of pH using a Zeta-sizer Nano-ZS (Malvern, UK). The pH values of GO aqueous dispersion were adjusted by 0.1 M HNO_3 or 0.1 M NaOH solution.

2.3. Zn(II) adsorption experiments

Batch adsorption experiments were carried out in 50 mL iodine flask containing GO stock solution (pH 5) and given Zn(II) concentration. Then, the suspension was mixed thoroughly by a mechanical shaker at an agitation speed of 170 rpm. Desired pH values in solution were adjusted by adding negligible volumes of 0.1 M HNO_3 or 0.1 M NaOH solution. After the adsorption equilibration was achieved, the solid phases were separated by centrifugation at 10,000 rpm for 5 min, and then filtered through a 0.22 μm filter membrane. Zn(II) concentration in the filtrate was determined by a Perkin-Elmer Analyst 700 atomic absorption spectrophotometer (AAS, Perkin-Elmer, USA).

Unless noted specifically, the following absorption experiments were conducted under the same condition. The effect of initial pH on Zn(II) removal was investigated over the pH range from 2.0 to 10.0. To investigate the kinetics of Zn(II) adsorption, 1 mL GO (2 mg/mL) was mixed with 30 mL Zn(II) solution at initial concentration of 40 mg/L, and the mixture (initial pH 7.0 ± 0.1) was stirred for a predetermined time intervals. The effect of adsorbent mass on the amount of Zn(II) adsorbed was obtained with a different adsorbent dose (2–10 mg) and the initial pH values in solution were controlled at 7.0 ± 0.1. The foreign ions effect ($NaNO_3$, NaCl and KCl) of Zn(II) adsorption was performed by the same above batch procedures except that different ionic strengths were used. Thermodynamic studies at different temperatures (20 °C, 30 °C, and 45 °C) were carried out by adding 2 mg adsorbent into 30 mL Zn(II) solution with different initial Zn(II) concentrations (10–100 mg/L).

All experiments were duplicated, and only the average values were reported. The maximum errors were less than 5%. The Zn(II) concentration retained in the adsorbent phase (q_e (mg/g)) was calculated from the difference between initial concentration and final equilibrium concentrations, as the following equation:

$$q_e = \frac{C_0 - C_e}{m} \times V \quad (1)$$

where C_0 and C_e are the initial and equilibrium concentrations of Zn(II) in solution (mg/L) respectively, V is the volume of solution (L), m is the adsorbent mass (g).

2.4. Zn(II) adsorption–desorption experiments

1 mL GO suspensions (2 mg/mL) were added to 30 mL Zn(II) solution (40 mg/L) and the mixture was shaken continuously at pH 7.0 ± 0.1 for 12 h. After reaching to equilibrium, GO was then withdrawn from the solution and the Zn(II) concentration of filtrate was determined. The spent GO were eluted by mixing the solid with 30 mL 0.1 M HNO_3, 0.1 M HCl and H_2O. After 24 h, the mixture was separated by centrifugation at 13,000 rpm for 20 min and then filtered through a 0.22 μm filter membrane.

3. Results and discussions

3.1. Graphene oxide characterization

Fig. 1 shows the SEM and AFM images of the prepared GO. As can be seen from Fig. 1a, it is obvious that GO is partially transparent with some crumples and has lateral dimensions of several micrometers with the small holes caused by overexposure to sonication. It suggests that the GO nanosheets may be prepared successfully [24]. According to AFM image (Fig. 1b), the thickness of GO nanosheets is about 6.48 nm (the inset table) for the selected place in the distribution graph. The above results demonstrate that few-layered GO nanosheets are formed because the thickness of monolayer graphene oxide is about 0.8–1.0 nm [23].

The XRD patterns of graphite powder and GO are exhibited in Fig. 2. The sharp diffraction peak of the graphite at $2\theta = 26.5°$ ($d = 0.31$ nm) corresponds to the normal graphite spacing of the graphite plane. After oxidation process in the synthesized GO, the characteristic graphite peak is disappeared. The broad and relatively weak diffraction peak is emerged at $2\theta = 10.9°$ with 0.81 nm d-spacing, corresponding to the typical diffraction peak of GO nanosheets [27]. The d-spacing increases from 0.31 to 0.81 nm after the graphite is converted into GO nanosheets, which may be due to the presence of plentiful oxygen-containing functional groups on the surface of GO. These groups result in an atomic-scale roughness GO [28]. The further proofs about the functional groups are offered by the following FT-IR analysis.

Fig. 3 presents the XPS spectra of graphite and graphene oxide. The wide scan XPS spectrum (Fig. 3b) of GO shows photoelectron lines at a binding energy of about 285.08 eV and 531.08 eV, attributed to C 1s, and O 1s, respectively. The quantitative analysis

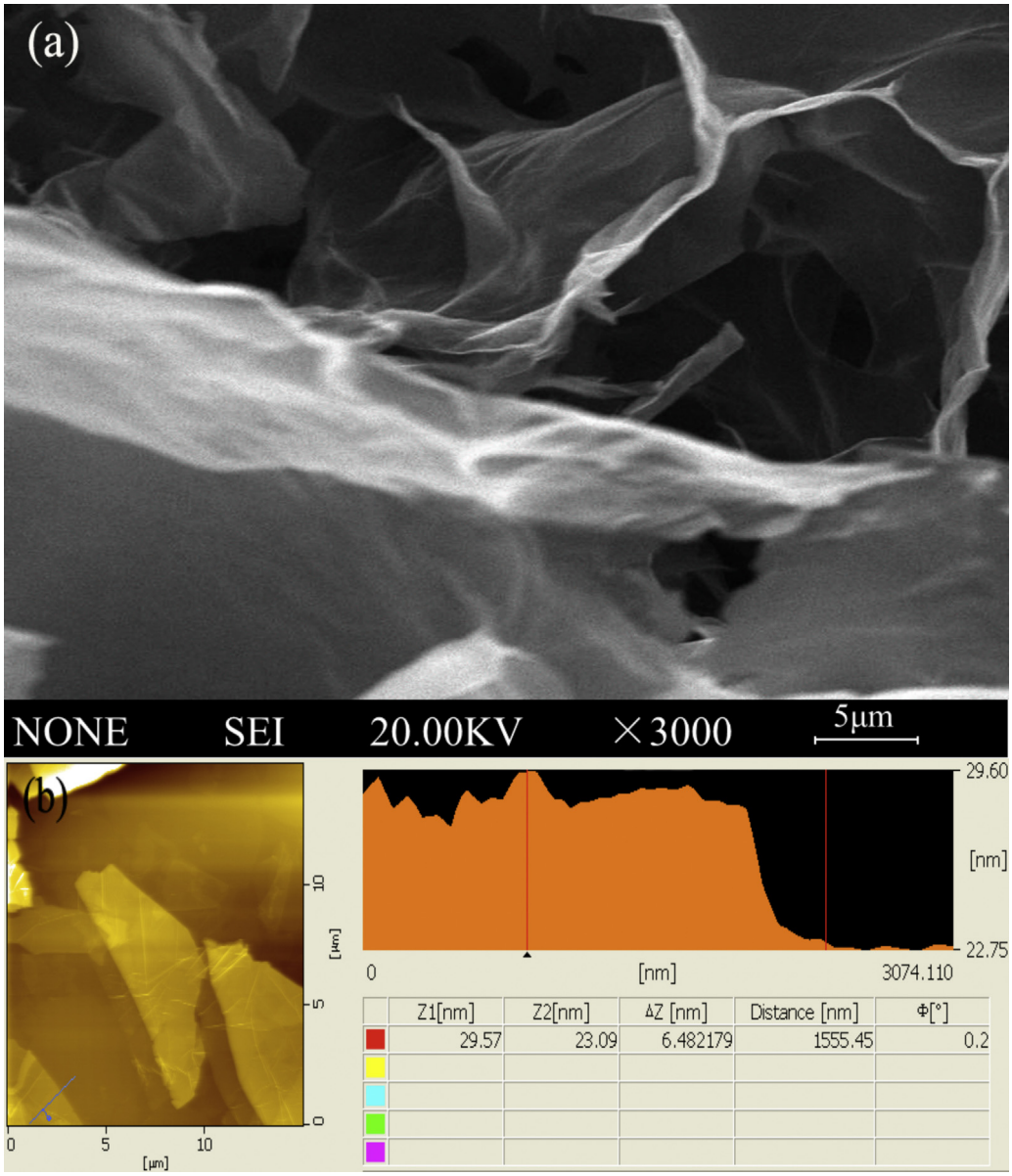

Fig. 1. The SEM image (a) and AFM image (b) of graphene oxide.

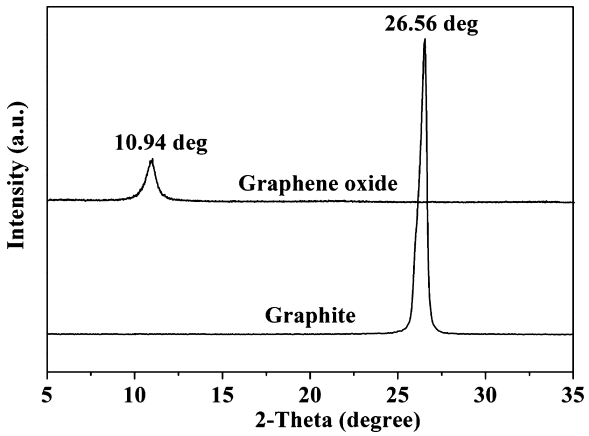

Fig. 2. The XRD patterns of graphite and graphene oxide.

shows that the ratio of carbon to oxygen (C/O) is about 10.40 (92.86 at% C and 8.93 at% O) in the graphite (Fig. 3a). After oxidation process, the presence of 66.43 at% of C and 31.51 at% of O (C/O = 2.11) indicates the high oxidation of the prepared GO by the modified Hummers' method [24].

The oxygen-containing groups on the surface of GO are characterized by FT-IR analysis (Fig. 4). Different functional groups are found in the FT-IR spectrum and it exhibits several characteristic peaks of O—H at 3407 cm^{-1}, C═O group at 1712 cm^{-1}, C═C at 1623 cm^{-1}, C—O group at 1222 cm^{-1}. It is indicated that abundant oxygen-containing functional groups exist on the surface of GO nanosheets.

Zeta potential was determined for prepared GO and the result shows that GO aqueous dispersion is pH-sensitive (Fig. 5). The surface charge of GO are highly negatively charged and zeta potential becomes more negative with the increase of pH within the pH range tested. This phenomenon may be due to the ionization of the different groups (carboxylic and/or hydroxyl group) on the surface of

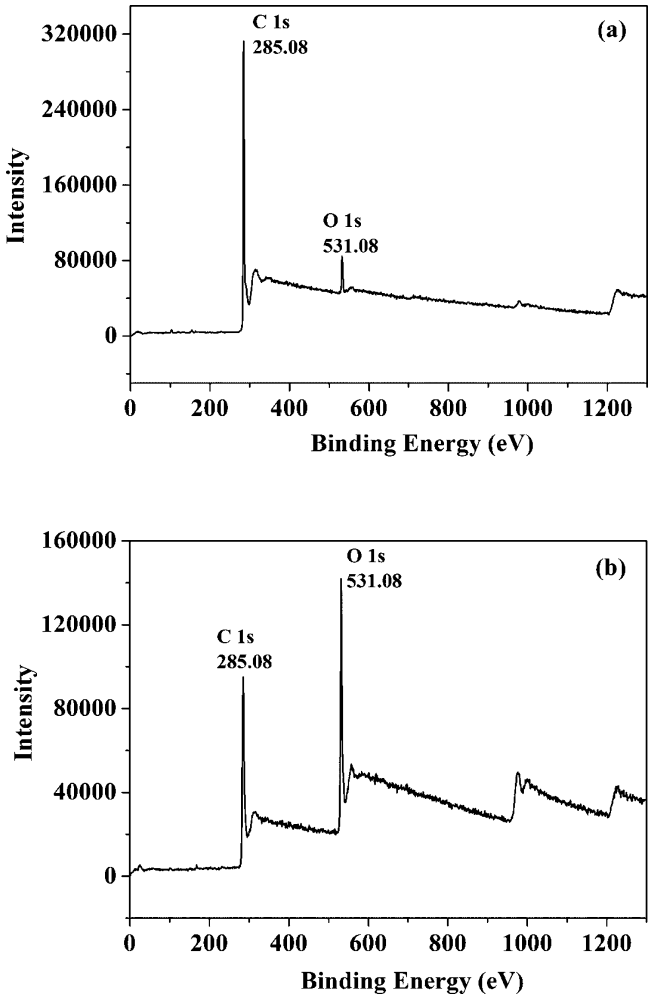

Fig. 3. The XPS spectra of graphite (a) and graphene oxide (b).

GO nanosheets [29]. It also suggests that stable GO colloid has been formed because of electrostatic repulsion [30].

3.2. Effect of initial pH on Zn(II) adsorption

Electrolyte pH plays a significant role in governing the adsorption behavior of Zn(II) on GO. As shown in Fig. 5, Zn(II) adsorption

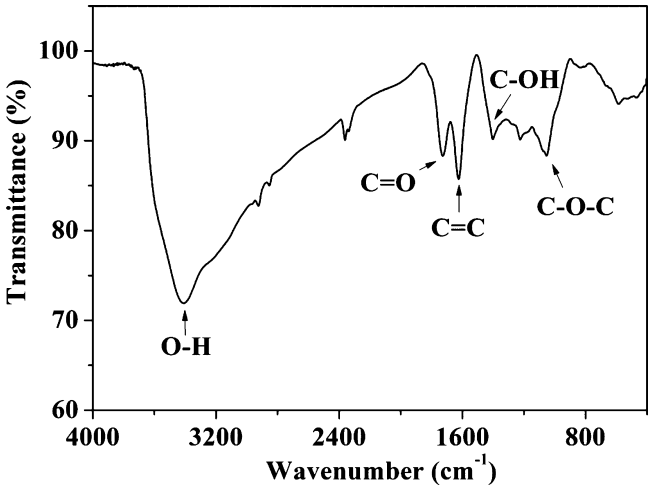

Fig. 4. The FT-IR spectrum of graphene oxide.

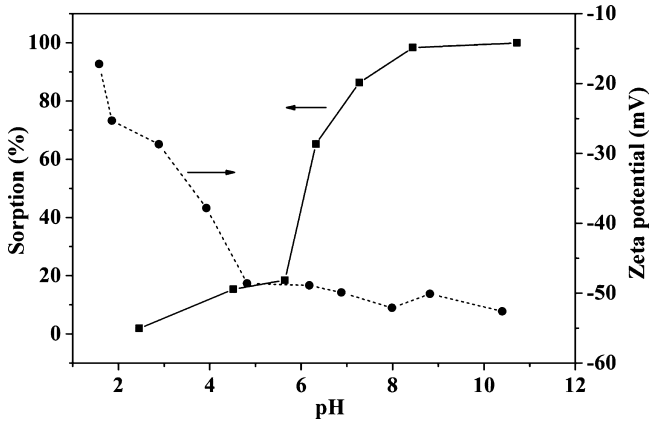

Fig. 5. Zeta potential of graphene oxide dispersion as a function of its pH value (●) and the effect of pH on removal efficiency by graphene oxide (■). $C[Zn(II)]_{initial}$ = 40 mg/L, $T = 20 \pm 0.1$ °C, m/V = 0.07 g/L.

depends greatly on pH and increases sharply with the increase of pH from 2.5 to 7.0, and reaches a maximum value above pH of 7.0. This fact may benefit from the ion exchange of Zn^{2+} with H^+ on GO surface during the adsorption process, and the exchanged H^+ ions are released to solution thereby leading to the decrease of pH values. Experiments have confirmed that the final pH values in solution after reaching adsorption equilibrium are lower than the initial pH values (Table 1). The similar phenomenon has been reported by Zhao et al. [24].

Generally, various Zn(II) species in aqueous solution are present in the form of Zn^{2+}, $Zn(OH)^+$, $Zn(OH)_2{}^0$, $Zn(OH)_3{}^-$ and $Zn(OH)_4{}^{2-}$ at a function of pH values [6]. At pH < 7.0, the predominant Zn(II) species is Zn^{2+} and the removal of Zn(II) is mainly accomplished by sorption reaction. Low removal efficiency is observed at the low pH range, which may be related with the fact that there are more protons in acid environment available to protonate active sites of GO surface, and the competition between zinc ion and H^+ occurred in solution [31]. At higher pH values, the lower concentration of H^+ and greater number of ligands with negatives charges lead to greater zinc adsorption. What's more, electrostatic attraction between positive zinc ion and negative surface of GO may offer another driving force to affect Zn(II) retention. However, in the pH range of 7.0–10.5, the removal of Zn(II) increased slowly and reached maximum with the efficiency of 99.3%. The main species are $Zn(OH)_2{}^0$, $Zn(OH)_3{}^-$ and $Zn(OH)_4{}^{2-}$ in aqueous solution, and thus simultaneous precipitation of $Zn(OH)_{2(s)}$ and adsorption of other zinc hydroxyl complex ions may be occurred. Similar phenomenon has also been shown in the adsorption of zinc ion from water with purified carbon nanotube [11]. In order to ensure no interference from metal precipitation during adsorption, the pH value in subsequent experiments were carried out at 7 ± 0.1.

3.3. Effect of foreign ions on the Zn(II) adsorption

Foreign ions are one of the key factors affecting the electrical double layer structure of hydrated particulate, which will impact the binding of adsorbing species [32]. Fig. 6 shows the amount of Zn adsorbed as affected by a different background electrolyte. The extent of Zn(II) adsorption decrease slightly with increasing $NaNO_3$, NaCl and KCl concentration from 0.001 to 0.01 mol/L in

Table 1
The initial and final pH in the adsorption system of Zn(II) onto GO.

Initial pH	2.45	4.51	5.64	6.32	7.27	8.44	10.72
Final pH	2.38	4.42	5.32	6.11	6.98	7.86	10.71

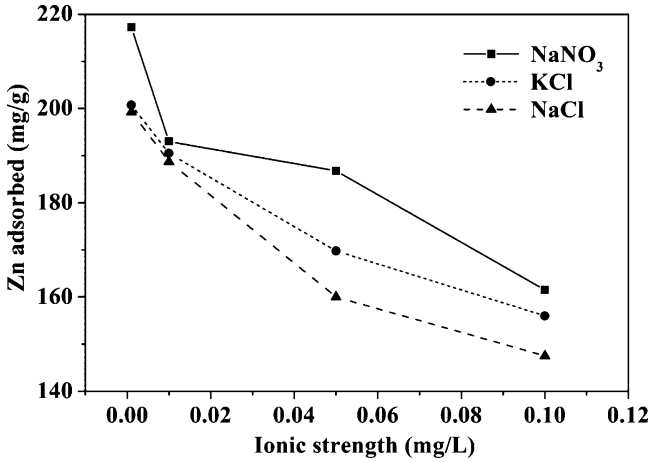

Fig. 6. Influence of foreign ions on the adsorption of Zn(II) on graphene oxide. $C[Zn(II)]_{initial}$ = 40 mg/L, T = 20 ± 0.1 °C, m/V = 0.07 g/L, pH 7.0 ± 0.1.

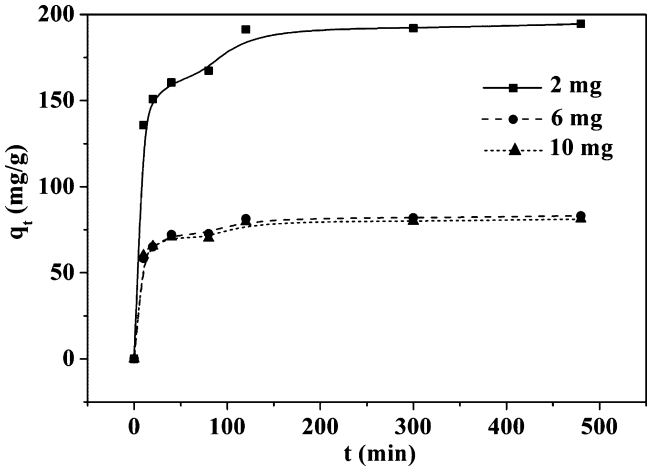

Fig. 7. Effect of contact time and adsorbent dosage on Zn(II) adsorption. $C[Zn(II)]_{initial}$ = 40 mg/L, T = 20 ± 0.1 °C, m/V = 0.07 g/L, pH 7.0 ± 0.1.

solution. These results indicate that ionic strength may influence the adsorption capacity of the adsorbent. This can be attributed in part to competition between Zn^{2+} and Na^+ and K^+ ions for the surface sites of GO as the ionic strength increase. In the presence of KCl, the adsorption of Zn(II) on GO is higher than that of NaCl, which may be due to that the radius of Na^+ is smaller than those of K^+, thus Na^+ has the higher affinity to the surface of GO and the higher tendency for counter-ion exchange with the surface groups of GO, which reduces ion interaction sites on the surface of GO with Zn(II). In contrast to $NaNO_3$, the adsorption capacity of GO for Zn(II) is lower in NaCl solution. This phenomenon may be ascribed to: (i) in the presence of Cl^- and NO_3^- in solution, complexing ligands between Zn^{2+} and Cl^- or NO_3^- are formed and may increase metal retention [33]. Compared with NO_3^-, Cl^- are highly mobile and have stronger complexing ability toward Zn^{2+} [34], which may reduce the adsorptive performance of GO. (ii) Cl^- is easily captured by the adjacent hydroxyl or carboxyl groups that are present on the GO, which may change the surface state of GO and decrease the availability of binding sites [35]. (iii) The inorganic acid radical radius order is $Cl^- < NO_3^-$. The smaller radium inorganic acid radicals takes up more ionic exchange sites, which may lead to the decrease of Zn(II) adsorption on GO. It is consistent with the compatibility obtained by Yang et al. [36] in the simulation of Ni(II) adsorption by oxidized multi-walled carbon nanotubes.

Moreover, outer-sphere complexes are more susceptible to the alterations of ionic strength than inner-sphere complexes since the background electrolyte ions are placed in the same plane [37]. Hayes et al. [38] concluded that β-plane sorption could be occurred when background electrolyte remarkably affects the sorption process; otherwise, o-plane sorption may proceed. Therefore, the above results imply that Zn(II) may participate in an β-plane complex reaction, which is affected by the background electrolyte (i.e., Na^+, K^+, Cl^-, NO_3^-). The pH and ionic strength-dependent indicate that an out-sphere surface complexation may contribute to the sorption of Zn(II) on GO.

3.4. Effect of adsorbent dosage on Zn(II) adsorption

Results of kinetic experiments with various GO concentrations are presented in Fig. 7. The amount of Zn(II) adsorbed per unit mass of adsorbent decrease as the adsorbent mass increase. Although the number of adsorption sites per unit mass of an adsorbent remains constant, independent of the total adsorbent mass, increasing the amount of adsorbent in a settled volume reduces the number of available sites as the effective surface area is likely to decrease [39]. Zinc ion can induce rapidly the aggregation/folding of GO by the strong interaction between Zn^{2+} and carboxyl groups [40]. With higher solid content, GO–GO interactions are perhaps physically hindering partial active sites from the adsorbing solutes and thus, causing decreased adsorption, or creating electrostatic interferences such that the electrical surface charges on the closely packed GO diminish attraction force between the adsorbing solute and surface of individual GO. Similar trends have also been reported in other adsorbents [41,42].

3.5. Effect of contact time on Zn(II) adsorption and adsorptive kinetics

Fig. 7 represents a plot of the amount of Zn(II) adsorbed (mg/g) versus contact time for various adsorbent concentrations. Obviously, Zn(II) adsorption increases with contact time and gradually reaches equilibrium for all samples. A rapid adsorption is observed within 20 min in that the availability of large number of vacant sites and the few-layered structure of GO. Subsequently, the diminishing availability of the remained active sites and the decrease in the driving force lead to the slow adsorptive process [43]. Similar results have been found by Wu et al. [26]. The rapid kinetics is important for GO to treat the practical wastewater, as it facilitates smaller reactor volumes, ensuring high efficiency and economy [42].

In order to explore the mechanism of adsorption, particularly the potential rate-controlling step, the transient behavior of Zn(II) adsorptive process is investigated using pseudo-first-order, pseudo-second-order, Elovich kinetic model and intra-particle diffusion model [26]. The correlation coefficient (R^2, close or equal to 1) is introduced to evaluate the suitability of different models. The linearized-integral forms of different kinetic models are expressed as:

$$\ln(q_e - q_t) = \ln\ q_e - \frac{k_1}{2.303}t \tag{2}$$

$$\frac{t}{q_t} = \frac{1}{2}k_2 q_e^2 + \frac{t}{q_e} \tag{3}$$

$$q_t = \beta \ln(\alpha\beta) + \beta \ln(t) \tag{4}$$

$$q_t = K_{id} t^{1/2} + C \tag{5}$$

where q_e and q_t (mg/g) are the values of amount adsorbed per unit mass at equilibrium and at instant of time t (min). k_1 (L/min) is the pseudo-first-order adsorption rate coefficient.

Table 2
Calculated kinetic parameters for pseudo first-order, second-order kinetic models, Elovich model for Zn(II) adsorption using GO as an adsorbent.

Adsorbent dosage (mg)	Pseudo-first-order model				Pseudo-second-order model				Elovich model		
	$q_{e,exp}$ (mg/g)	k_1 (1 min^{-1})	$q_{e,cal}$ (mg/g)	R^2	$q_{e,exp}$ (mg/g)	k_2 (1 min^{-1})	$q_{e,cal}$ (mg/g)	R^2	α	β	R^2
2	196	0.009	58	0.780	196	1.59×10^{-6}	196	0.999	106	0.034	0.832
6	84	0.009	23	0.792	84	1.80×10^{-5}	84	0.999	49	0.079	0.818
10	81	0.010	23	0.818	81	1.89×10^{-5}	82	0.999	54	0.083	0.785

k_2 (g/(mg min)) is the pseudo-second-order rate coefficient. The Elovich coefficients, α and β, represent the initial adsorption rate (g/(mg min^2) and the desorption coefficient (mg/(g min) respectively. K_{id} (mg/(g min$^{1/2}$)) is the diffusion rate coefficient. C is the intercept and relate to the thickness of the boundary layer.

The fitting curves resulting from the linearized-integral form of pseudo-first-order, pseudo-second-order and Elovich kinetic model are plotted in Fig. 8. The parameter values for each system are calculated from the linear least square method and the results are presented in Table 2 along with the correlation coefficient. It can be seen that pseudo-second-order kinetic model provides a good correlation (R^2, close to 1) for the adsorption of Zn(II) on the GO sample. What is more, the q_e values, calculated by pseudo-second-order model, represent a fine agreement with the detected values in experiment. Therefore, the pseudo-second-order kinetic model is able to describe properly the kinetic behavior of Zn(II) adsorption on GO. Meanwhile, it is also suggested that an assumption behind the pseudo-second-order model that the rate-limiting step of Zn(II) uptake process is the consequence of chemisorption and more than one-step may be involved in sorption processes [42]. Analogous results had also been acquired by many researchers for different systems [21,44].

For a solid/liquid sorption process or the design of adsorption systems, it is helpful to elaborate the underlying adsorption mechanism by analyzing the rate controlling steps, such as mass transport and chemical reaction processes. In general, adsorption reaction may be considered the following steps [43]: (i) the migration and diffusion of metal ions from the boundary film to the external surface of the adsorbent (film diffusion); (ii) transfer of metal ions into the intraparticular active sites (particle diffusion); (iii) adsorption of metal ions at the active sites of adsorbent. Currently, intra-particle diffusion model is widely used to predict the rate controlling step.

The plots of q_t versus $t^{1/2}$ at different adsorbent concentrations are shown in Fig. 9. And the intraparticle diffusion parameters and the determination coefficients are summarized in Table 3. Apparently, these plots are nonlinear over the whole time range and show multilinearity characterization. The first sharp section can be act as the diffusion of Zn(II) through the solution to the external surface of GO or the boundary surface diffusion of the sorbate. The second subdued portion is the slow adsorption stage, where intraparticle diffusion is rate-controlled [45]. However, it can be found that none of plots give linear straight line passing through the origin ($C \neq 0$) (Table 3). So the intraparticle diffusion is involved but not the only rate controlling step for the adsorption of Zn(II) onto GO.

Table 3
Calculated kinetic parameters for intraparticle diffusion model for Zn(II) adsorption on GO.

Adsorbent dosage (mg)	Intraparticle diffusion model		
	K_{id} (mg/g min$^{1/2}$)	C	R^2
2	2.97	139.3	0.753
6	1.18	61.2	0.708
10	1.03	61.7	0.740

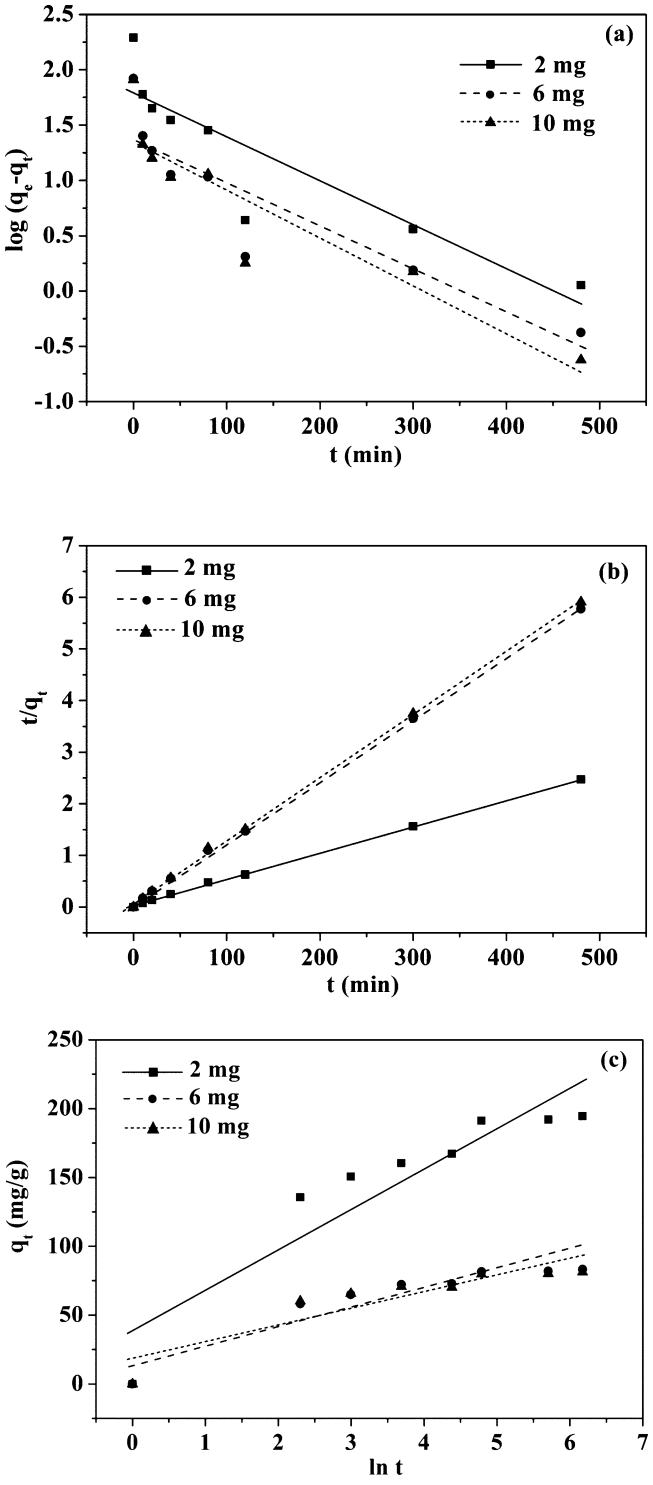

Fig. 8. Pseudo-first-order kinetic model (a), pseudo-second-order kinetic model (b) and Elovich kinetic model (c) for Zn(II) adsorption at different adsorbent concentrations. $C[Zn(II)]_{initial}$ = 40 mg/L, T = 20 ± 0.1 °C, m/V = 0.07 g/L, pH 7.0 ± 0.1.

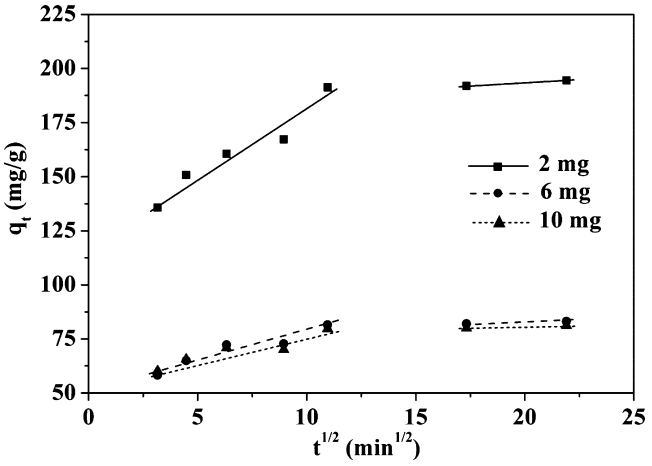

Fig. 9. Intra-particle diffusion model for Zn(II) adsorption at different adsorbent concentrations. $C[Zn(II)]_{initial}$ = 40 mg/L, T = 20 ± 0.1 °C, m/V = 0.07 g/L, pH 7.0 ± 0.1.

3.6. Effect of temperature and adsorption isotherm

In order to study the influence of temperature, experiments at 20 °C, 30 °C and 45 °C were accomplished and the results are presented in Fig. 10. It has been discovered that the absorption process is more favorable at lower temperature. This is mainly because of decreased surface activity implying that absorption between Zn^{2+} ion and GO is an exothermal reaction. With increasing temperature, the attractive forces between the graphene oxide surface and Zn^{2+} are weakened and then sorption decreases. Sen et al. [42] has also obtained similar type's result for a different adsorbent system.

Adsorption isotherm can provide the most important parameter for designing a desired adsorption system. In this study, the Freundlich (Eq. (7)) and Langmuir (Eq. (8)) isotherms are adopted to describe the adsorption behaviors of Zn(II) onto GO. The linear equations are as follows:

$$\ln\ q_e = \ln k_F + \frac{1}{n}\ln C_e \tag{7}$$

$$\frac{C_e}{q_e} = \frac{C_e}{q_{max}} + \frac{k_L}{q_{max}} \tag{8}$$

where k_F is Freundlich constant (L/mg), which indicates the relative adsorption capacity of the adsorbent; n is the heterogeneity factor and is known as Freundlich coefficient; q_{max} is the maximal sorption capacity at equilibrium (mg/g); k_L is Langmuir constant

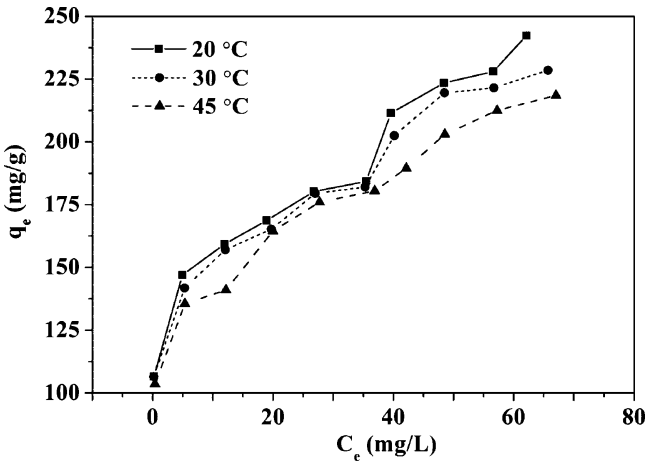

Fig. 10. Effect of temperature on the adsorption of Zn(II) onto graphene oxide. $C[Zn(II)]_{initial}$ = 10–100 mg/L, m/V = 0.07 g/L, pH 7.0 ± 0.1.

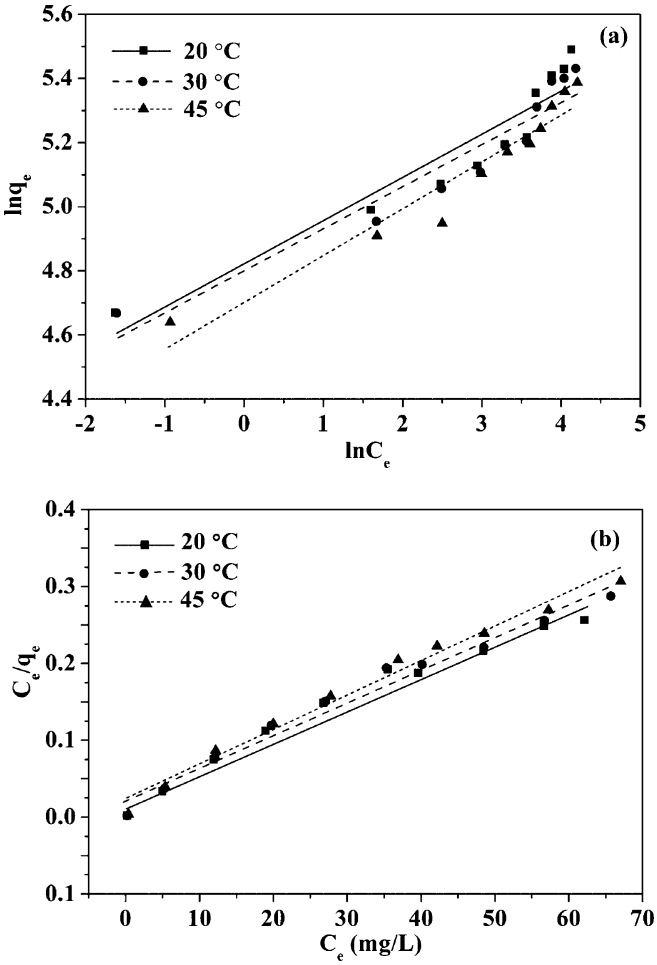

Fig. 11. Freundlich adsorption isotherm (a) and Langmuir adsorption isotherm (b) for Zn(II) adsorption onto graphene oxide. $C[Zn(II)]_{initial}$ = 10–100 mg/L, m/V = 0.07 g/L, pH 7.0 ± 0.1.

related to the affinity of the binding sites and energy of adsorption (L/g);

Fig. 11a shows the Freundlich isotherm fittings for GO with poor regression coefficient (Table 4) when ln q_e is plotted against ln C_e. The values of 'n', evaluated from the slope, are larger than 1 and decrease as the temperature increases. This phenomenon indicates the favorable nature of adsorption at lower temperature [26].

Fig. 11b gives results on Langmuir isotherm fittings for GO adsorbent. The maximum adsorption capacity of Zn(II), q_{max} and Langmuir constant, k_L is 246 mg/g and 5.7, respectively at the temperature of 20 °C for Zn–GO system. From Table 4, the high values of regression coefficient (R^2) indicate a good agreement between the isotherm parameters and experimental values. Meanwhile, a dimensionless constant (R_L) called separation factor has been calculated from Langmuir plot by the following equation [46]:

$$R_L = \frac{1}{1 + k_L C_0} \tag{9}$$

where C_0 is the highest initial concentration (mg/L) in the liquid phase.

It can be found from Table 4 that the range of R_L (Table 4) is 2.11×10^{-3} to 2.25×10^{-3}, which gives favorable adsorption as it lies in 0–1. From Fig 11a and b, it is also seen that Langmuir isotherms fit better with experimental data than Freundlich isotherms. This also suggests that Zn(II) adsorption on GO maybe monolayer coverage.

Table 4
Isotherm constants and regression data for various adsorption isotherms for adsorption of Zn(II) on GO.

Temperature (°C)	Langmuir				Freundlich		
	q_{max} (mg/g)	k_L (L/g)	R^2	R_L	$1/n$	k_F (L/g)	R^2
20	246	5.70	0.967	2.11×10^{-3}	0.135	1.572	0.885
30	236	5.39	0.977	2.23×10^{-3}	0.130	1.570	0.895
45	225	5.35	0.981	2.25×10^{-3}	0.145	1.549	0.920

3.7. Thermodynamics study

Thermodynamic parameters involving Gibbs free energy (ΔG°), enthalpy change (ΔH°) and change in entropy (ΔS°) are obtained at different temperatures according to the following formulas [47]:

$$\Delta G^\circ = -RT \ln b \quad (10)$$

$$\Delta H^\circ = -R \frac{T_2 T_1}{T_2 - T_1} \ln \left(\frac{b_2}{b_1} \right) \quad (11)$$

$$\Delta S^\circ = \frac{\Delta H^\circ - \Delta G^\circ}{T} \quad (12)$$

where R (8.314 J/mol K) is the ideal gas constant, T (K) is the absolute temperature, and b is Langmuir constant (the unit should be transformed into milligrams per gram for the calculation of ΔG°) at a specific temperature. All these thermodynamic parameters are listed in Table 5.

The obtained values of energy ΔG° are from −37.89 to −40.96. The negative values at three tested temperatures reveal that the adsorption process is feasible and spontaneous, and the adsorption is a physisorption and chemisorption process simultaneously [26]. According to the negative value of ΔH°, it infers that the adsorption reaction is exothermic in nature and the adsorption process is energetically stable. The positive ΔS° values suggest the increased randomness at the solid/solution interface during the adsorption process. Analogous thermodynamic parameters are also reported for the Zn(II) adsorption onto other sorbents from aqueous solution [32,42,48].

3.8. Desorption study

The adsorption–desorption experiments are carried out to explore the possibility of recycling of GO and recovery of Zn(II) ions. Desorption of Zn(II) from GO is investigated using three different eluent buffers. The desorption percentages of Zn(II) eluted from the spent graphene oxide are 91.6%, 73.4% and 53.2% with using 0.1 M HCl, 0.1 M HNO_3 and H_2O, respectively. However, complexing agents, including ethylenediaminetetraacetic acid and ethylene diamine, may be much more effective for Zn(II) desorption. Therefore, a systematic study about the other optimum conditions such as eluting agents, pH, desorption time, temperature and recycling should be progressed.

Table 5
Thermodynamic parameters for Zn(II) adsorbed by GO.

Temperature (°C)	ΔG° (kJ/mol)	ΔS° (kJ/(K mol))	ΔH° (kJ/mol)
20	−37.89	0.137	−2.171
30	−39.44	0.136	
45	−40.96	0.134	

The value of ΔH° listed is an average one.

Table 6
Comparison of Zn(II) removal with different adsorbents reported in literature.

Adsorbent	Adsorption capacities (mg/g)	Reference
Modified carbon nanofibers	1.05	[10]
Purified carbon nanotubes	43.66	[11]
Modified multiwalled carbon nanotubes	32.68	[12]
Nanoporous carbon	130.76	[49]
Commercial activated carbon	40.86	[49]
Ice husk	19.38	[50]
Activated carbon	22.03	[51]
Magnesium/activated carbon	9.68	[52]
Carbon nanotube sheets	74.63	[53]
γ-Al_2O_3	7.60	[54]
Hematite nanoparticles	8.56	[55]
Carrot residues	29.61	[56]
Carbon aerogel	1.18	[57]
Graphene oxide	246	This study

3.9. Comparison of Zn(II) removal with different adsorbents reported in literature

Adsorption capacity of other adsorbents for the removal of Zn(II) from aqueous phase is given in Table 6 for comparison. In view of favorable characteristics of GO, it is obvious that graphene oxide is an effective adsorbent for eliminating Zn(II) from effluents.

4. Conclusions

Graphene oxide was prepared from powder graphite by using the modified Hummers' method. The adsorption of Zn(II) on GO was strongly dependent on pH and also weakly affected by foreign ions and ionic strength. The amount of Zn(II) adsorption on GO decreased with the increase of adsorbent dosage. The Zn(II) adsorption process followed the pseudo-second-order kinetics. Equilibrium data at different temperatures were described well with Langmuir isotherms, suggesting that the adsorption process was mainly monolayer. The main strength of adsorption was the chemical adsorption such as ion exchange, while the electrostatic interaction could also contribute to the whole interaction. The thermodynamic parameters obtained from the temperature dependent adsorption isotherms indicated that the adsorption reaction was a spontaneous and exothermic process in nature. Hydrochloric acid might be the suitable eluent buffer for the zinc ion desorption from Zn(II)-loaded graphene oxide.

Acknowledgments

The authors gratefully acknowledge the financial support provided by the National Water Pollution Control and Management Technology Major Project of China (No. 2009ZX07212-001-02), the National Natural Science Foundation of China (No. 21276069), and the Fundamental Research Funds for the Central Universities.

References

[1] Z. Xiao, R. Zhang, X. Chen, X. Li, T. Zhou, Magnetically recoverable Ni@carbon nanocomposites: solid-state synthesis and the application as excellent adsorbents for heavy metal ions, Applied Surface Science 263 (2012) 795–803.

[2] H.N. Bhatti, B. Mumtaz, M.A. Hanif, R. Nadeem, Removal of Zn(II) ions from aqueous solution using *Moringa oleifera* Lam. (horseradish tree) biomass, Process Biochemistry 42 (2007) 547–553.
[3] S. Tunali, T. Akar, Zn(II) biosorption properties of *Botrytis cinerea* biomass, Journal of Hazardous Materials 131 (2006) 137–145.
[4] A.K. Bhattacharya, S.N. Mandal, S.K. Das, Adsorption of Zn(II) from aqueous solution by using different adsorbents, Chemical Engineering Journal 123 (2006) 43–51.
[5] M. Barczak, E. Skwarek, W. Janusz, A. Dąbrowski, S. Pikus, Functionalized SBA-15 organosilicas as sorbents of zinc(II) ions, Applied Surface Science 256 (2010) 5370–5375.
[6] H. Zhang, Z. Tong, T. Wei, Y. Tang, Removal characteristics of Zn(II) from aqueous solution by alkaline Ca-bentonite, Desalination 276 (2011) 103–108.
[7] C. Chang, Q.D. Truong, J. Chen, Graphene sheets synthesized by ionic-liquid-assisted electrolysis for application in water purification, Applied Surface Science 264 (2013) 329–334.
[8] I. Ali, V.K. Gupta, Advances in water treatment by adsorption technology, Nature Protocols 1 (2006) 2661–2667.
[9] L.S. Ferreira, M.S. Rodrigues, J.C.M. de Carvalho, A. Lodi, E. Finocchio, P. Perego, A. Converti, Adsorption of Ni^{2+}, Zn^{2+} and Pb^{2+} onto dry biomass of *Arthrospira (Spirulina) platensis* and *Chlorella vulgaris*. I. Single metal systems, Chemical Engineering Journal 173 (2011) 326–333.
[10] M.A. Atieh, Effect of functionalized carbon nanofibers with carboxylic function group on the removal of zinc from water, IJESD 2 (2011) 142–145.
[11] C. Lu, H. Chiu, Adsorption of zinc(II) from water with purified carbon nanotubes, Chemical Engineering Science 61 (2006) 1138–1145.
[12] C. Lu, H. Chiu, Chemical modification of multiwalled carbon nanotubes for sorption of Zn^{2+} from aqueous solution, Chemical Engineering Journal 139 (2008) 462–468.
[13] R.L. Ramos, L.A.B. Jacome, J.M. Barron, L.F. Rubio, R.M.G. Coronado, Adsorption of zinc(II) from an aqueous solution onto activated carbon, Journal of Hazardous Materials B90 (2002) 27–38.
[14] Y. Zhang, Y. Li, L.Q. Yang, X.J. Ma, L.Y. Wang, Z.F. Ye, Characterization and adsorption mechanism of Zn^{2+} removal by PVA/EDTA resin in polluted water, Journal of Hazardous Materials 178 (2010) 1046–1054.
[15] M.S. Mauter, M. Elimelech, Environmental applications of carbon-based nanomaterials, Environmental Science and Technology 42 (2008) 5843–5859.
[16] G. Zhao, T. Wen, C. Chen, X. Wang, Synthesis of graphene-based nanomaterials and their application in energy-related and environmental-related areas, RSC Advances 2 (2012) 9286.
[17] X. Huang, X. Qi, F. Boey, H. Zhang, Graphene-based composites, Chemical Society Reviews 41 (2012) 666–686.
[18] H. Wang, X. Yuan, Y. Wu, H. Huang, X. Peng, G. Zeng, H. Zhong, J. Liang, M. Ren, Graphene-based materials: fabrication, characterization and application for the decontamination of wastewater and wastegas and the hydrogen storage/generation, Advances in Colloid and Interface Science (2013), http://dx.doi.org/10.1016/j.cis.2013.03.009.
[19] D.R. Dreyer, S. Park, C.W. Bielawski, R.S. Ruoff, The chemistry of graphene oxide, Chemical Society Reviews 39 (2010) 228–240.
[20] S. Stankovich, D.A. Dikin, G.H. Dommett, K.M. Kohlhaas, E.J. Zimney, E.A. Stach, R.D. Piner, S.T. Nguyen, R.S. Ruoff, Graphene-based composite materials, Nature 442 (2006) 282–286.
[21] S.T. Yang, S. Chen, Y. Chang, A. Cao, Y. Liu, H. Wang, Removal of methylene blue from aqueous solution by graphene oxide, Journal of Colloid and Interface Science 359 (2011) 24–29.
[22] Y. Gao, Y. Li, L. Zhang, H. Huang, J. Hu, S.M. Shah, X. Su, Adsorption and removal of tetracycline antibiotics from aqueous solution by graphene oxide, Journal of Colloid and Interface Science 368 (2012) 540–546.
[23] G. Zhao, J. Li, X. Ren, C. Chen, X. Wang, Few-layered graphene oxide nanosheets as superior sorbents for heavy metal ion pollution management, Environmental Science and Technology 45 (2011) 10454–10462.
[24] G. Zhao, X. Ren, X. Gao, X. Tan, J. Li, C. Chen, Y. Huang, X. Wang, Removal of Pb(II) ions from aqueous solutions on few-layered graphene oxide nanosheets, Dalton Transactions 40 (2011) 10945–10952.
[25] S. Liu, K. Chen, Y. Fu, S. Yu, Z. Bao, Reduced graphene oxide paper by supercritical ethanol treatment and its electrochemical properties, Applied Surface Science 258 (2012) 5299–5303.
[26] Y. Wu, H. Luo, H. Wang, C. Wang, J. Zhang, Z. Zhang, Adsorption of hexavalent chromium from aqueous solutions by graphene modified with cetyltrimethylammonium bromide, Journal of Colloid and Interface Science 394 (2013) 183–191.
[27] W. Ma, J. Li, B. Deng, X. Zhao, Preparation and characterization of long-chain alkyl silane-functionalized graphene film, Journal of Materials Science 48 (2013) 156–161.
[28] L. Ai, C. Zhang, Z. Chen, Removal of methylene blue from aqueous solution by a solvothermal-synthesized graphene/magnetite composite, Journal of Hazardous Materials 192 (2011) 1515–1524.
[29] X. Hu, Y. Yu, W. Hou, J. Zhou, L. Song, Effects of particle size and pH value on the hydrophilicity of graphene oxide, Applied Surface Science (2013), http://dx.doi.org/10.1016/j.apsusc.2013.01.201.
[30] D. Li, M.B. Muller, S. Gilje, R.B. Kaner, G.G. Wallace, Processable aqueous dispersions of graphene nanosheets, Nature Nanotechnology 3 (2008) 101–105.
[31] C.P. Jordao, R.B.A. Fernandes, K.D.L. Ribeiro, B.D.S. Nascimento, P.M.D. Barros, Zn(II) adsorption from synthetic solution and kaolin wastewater onto vermicompost, Journal of Hazardous Materials 162 (2009) 804–811.
[32] C. Weng, C. Huang, Adsorption characteristics of Zn(II) from dilute aqueous solution by fly ash, Colloids and Surfaces A: Physicochemical and Engineering Aspects 247 (2004) 137–143.
[33] C.C. Pye, C.R. Corbeil, W.W. Rudolph, An ab initio investigation of zinc chloro complexes, Physical Chemistry Chemical Physics 8 (2006) 5428–5436.
[34] A. Ghallab, A.R.A. Usman, Effect of sodium chloride-induced salinity on phyto-availability and speciation of Cd in soil solution, Water, Air, and Soil Pollution 185 (2007) 43–51.
[35] X. Zhou, Y. Wei, Q. He, F. Boey, Q. Zhang, H. Zhang, Reduced graphene oxide films used as matrix of MALDI-TOF-MS for detection of octachlorodibenzo-p-dioxin, Chemical Communications 46 (2010) 6974–6976.
[36] S. Yang, J. Li, D. Shao, J. Hu, X. Wang, Adsorption of Ni(II) on oxidized multi-walled carbon nanotubes: effect of contact time, pH, foreign ions and PAA, Journal of Hazardous Materials 166 (2009) 109–116.
[37] J. Li, S. Zhang, C. Chen, G. Zhao, X. Yang, J. Li, X. Wang, Removal of Cu(II) and fulvic acid by graphene oxide nanosheets decorated with Fe_3O_4 nanoparticles, ACS Applied Materials and Interfaces 4 (2012) 4991–5000.
[38] K.F. Hayes, J.O. Leckie, Modeling ionic strength effects on cation adsorption at hydrous oxide/solution interfaces, Journal of Colloid and Interface Science 115 (1987) 564–572.
[39] T.K. Sen, M.V. Sarzali, Removal of cadmium metal ion (Cd^{2+}) from its aqueous solution by aluminium oxide (Al_2O_3): a kinetic and equilibrium study, Chemical Engineering Journal 142 (2008) 256–262.
[40] S.T. Yang, Y. Chang, H. Wang, G. Liu, S. Chen, Y. Wang, Y. Liu, A. Cao, Folding/aggregation of graphene oxide and its application in Cu^{2+} removal, Journal of Colloid and Interface Science 351 (2010) 122–127.
[41] F. Arias, T.K. Sen, Removal of zinc metal ion (Zn^{2+}) from its aqueous solution by kaolin clay mineral: A kinetic and equilibrium study, Colloids and Surfaces A: Physicochemical and Engineering Aspects 348 (2009) 100–108.
[42] T.K. Sen, D. Gomez, Adsorption of zinc (Zn^{2+}) from aqueous solution on natural bentonite, Desalination 267 (2011) 286–294.
[43] Y. Li, Q. Du, T. Liu, J. Sun, Y. Jiao, Y. Xia, L. Xia, Z. Wang, W. Zhang, K. Wang, H. Zhu, D. Wu, Equilibrium, kinetic and thermodynamic studies on the adsorption of phenol onto graphene, Materials Research Bulletin 47 (2012) 1898–1904.
[44] G.K. Ramesha, A.V. Kumara, H.B. Muralidhara, S. Sampath, Graphene and graphene oxide as effective adsorbents toward anionic and cationic dyes, Journal of Colloid and Interface Science 361 (2011) 270–277.
[45] M. Omraei, H. Esfandian, R. Katal, M. Ghorbani, Study of the removal of Zn(II) from aqueous solution using polypyrrole nanocomposite, Desalination 271 (2011) 248–256.
[46] W.W. Tang, G.M. Zeng, J.L. Gong, Y. Liu, X.Y. Wang, Y.Y. Liu, Z.F. Liu, L. Chen, X.R. Zhang, D.Z. Tu, Simultaneous adsorption of atrazine and Cu (II) from wastewater by magnetic multi-walled carbon nanotube, Chemical Engineering Journal 211-212 (2012) 470–478.
[47] P.H.T. Ren, W. Niu, Y. Wu, L. Ai, X. Gou, Synthesis of α-Fe_2O_3 nanofibers for applications in removal and recovery of Cr(VI) from wastewater, Environmental Science and Pollution Research 20 (2013) 155–162.
[48] V. Boonamnuayvitaya, C. Chaiya, W. Tanthapanichakoon, S. Jarudilokkul, Removal of heavy metals by adsorbent prepared from pyrolyzed coffee residues and clay, Separation and Purification Technology 35 (2004) 11–22.
[49] J.P. Ruparelia, S.P. Duttagupta, A.K. Chatterjee, S. Mukherji, Potential of carbon nanomaterials for removal of heavy metals from water, Desalination 232 (2008) 145–156.
[50] E.I. El-Shafey, Removal of Zn(II) and Hg(II) from aqueous solution on a carbonaceous sorbent chemically prepared from rice husk, Journal of Hazardous Materials 175 (2010) 319–327.
[51] H. Kalavathy, B. Karthik, L.R. Miranda, Removal and recovery of Ni and Zn from aqueous solution using activated carbon from *Hevea brasiliensis*: batch and column studies, Colloids and Surfaces B: Biointerfaces 78 (2010) 291–302.
[52] H. Yanagisawa, Y. Matsumoto, M. Machida, Adsorption of Zn(II) and Cd(II) ions onto magnesium and activated carbon composite in aqueous solution, Applied Surface Science 256 (2010) 1619–1623.
[53] M.A. Tofighy, T. Mohammadi, Adsorption of divalent heavy metal ions from water using carbon nanotube sheets, Journal of Hazardous Materials 185 (2011) 140–147.
[54] Y.J.O. Asencios, M.R. Sun-Kou, Synthesis of high-surface-area γ-Al_2O_3 from aluminum scrap and its use for the adsorption of metals: Pb(II), Cd(II) and Zn(II), Applied Surface Science 258 (2012) 10002–10011.
[55] V.A. Grover, J. Hu, K.E. Engates, H.J. Shipley, Adsorption and desorption of bivalent metals to hematite nanoparticles, Environmental Toxicology and Chemistry 31 (2012) 86–92.
[56] B. Nasernejad, T.E. Zadeh, B.B. Pour, M.E. Bygi, A. Zamani, Comparison for biosorption modeling of heavy metals (Cr(III), Cu(II), Zn(II)) adsorption from wastewater by carrot residues, Process Biochemistry 40 (2005) 1319–1322.
[57] A.K. Meena, G.K. Mishra, P.K. Rai, C. Rajagopal, P.N. Nagar, Removal of heavy metal ions from aqueous solutions using carbon aerogel as an adsorbent, Journal of Hazardous Materials 122 (2005) 161–170.